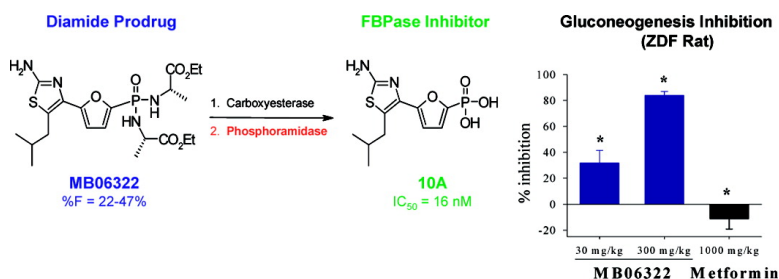


Discovery of Potent and Specific Fructose-1,6-Bisphosphatase Inhibitors and a Series of Orally-Bioavailable Phosphoramidase-Sensitive Prodrugs for the Treatment of Type 2 Diabetes

Qun Dang, Srinivas Rao Kasibhatla, K. Raja Reddy, Tao Jiang, M. Rami Reddy, Scott C. Potter, James M. Fujitaki, Paul D. van Poelje, Jingwei Huang, William N. Lipscomb, and Mark D. Erion

J. Am. Chem. Soc., **2007**, 129 (50), 15491-15502 • DOI: 10.1021/ja074871l

Downloaded from <http://pubs.acs.org> on February 9, 2009



More About This Article

Additional resources and features associated with this article are available within the HTML version:

- Supporting Information
- Links to the 5 articles that cite this article, as of the time of this article download
- Access to high resolution figures
- Links to articles and content related to this article
- Copyright permission to reproduce figures and/or text from this article

[View the Full Text HTML](#)

Discovery of Potent and Specific Fructose-1,6-Bisphosphatase Inhibitors and a Series of Orally-Bioavailable Phosphoramidase-Sensitive Prodrugs for the Treatment of Type 2 Diabetes

Qun Dang,[†] Srinivas Rao Kasibhatla,^{†,‡} K. Raja Reddy,[†] Tao Jiang,^{†,§} M. Rami Reddy,[†] Scott C. Potter,[†] James M. Fujitaki,[†] Paul D. van Poelje,[†] Jingwei Huang,^{||} William N. Lipscomb,^{||} and Mark D. Erion^{*,†}

Contribution from the Departments of Medicinal Chemistry, Biochemistry, and Molecular Modeling, Metabasis Therapeutics, Inc., La Jolla, California 92037, and Department of Chemistry and Chemical Biology, Harvard University, Cambridge, Massachusetts 02138

Received July 3, 2007; E-mail: erion@mbasis.com

Abstract: Excessive glucose production by the liver coupled with decreased glucose uptake and metabolism by muscle, fat, and liver results in chronically elevated blood glucose levels in patients with type 2 diabetes. Efforts to treat diabetes by reducing glucose production have largely focused on the gluconeogenesis pathway and rate-limiting enzymes within this pathway such as fructose-1,6-bisphosphatase (FBPase). The first potent FBPase inhibitors were identified using a structure-guided drug design strategy (Erion, M. D.; et al. *J. Am. Chem. Soc.* **2007**, *129*, 15480–15490) but proved difficult to deliver orally. Herein, we report the synthesis and characterization of a series of orally bioavailable FBPase inhibitors identified following the combined discoveries of a low molecular weight inhibitor series with increased potency and a phosphonate prodrug class suitable for their oral delivery. The lead inhibitor, **10A**, was designed with the aid of X-ray crystallography and molecular modeling to bind to the allosteric AMP binding site of FBPase. High potency ($IC_{50} = 16$ nM) and FBPase specificity were achieved by linking a 2-aminothiazole with a phosphonic acid. Free-energy perturbation calculations provided insight into the factors that contributed to the high binding affinity. **10A** and standard phosphonate prodrugs of **10A** exhibited poor oral bioavailability (0.2–11%). Improved oral bioavailability (22–47%) was achieved using phosphonate diamides that convert to the corresponding phosphonic acid by sequential action of an esterase and a phosphoramidase. Oral administration of the lead prodrug, MB06322 (**30**, CS-917), to Zucker Diabetic Fatty rats led to dose-dependent inhibition of gluconeogenesis and endogenous glucose production and consequently to significant blood glucose reduction.

Introduction

Type 2 diabetes mellitus (T2DM) is a growing worldwide health concern that is expected to afflict over 366 million people by 2030.¹ Patients with diabetes exhibit chronically elevated blood glucose levels and, as a consequence, are at increased risk of long-term complications arising from glucose-mediated damage to organs such as the eyes, kidneys, nerves, heart, and blood vessels. Numerous drug classes are available that lower glucose levels and reduce diabetic complications.² Unfortunately, the glucose-lowering effect usually diminishes over time due to poor compliance, suboptimal dose titration, decreased

pancreatic function, and exacerbation of peripheral insulin resistance, leaving the majority of treated patients with fasting and postprandial glucose levels above the target levels.³ Consequently, there remains a large need for new, more effective, and longer-acting drugs to treat T2DM.

Blood glucose levels are elevated in T2DM due to reduced glucose metabolism by tissues such as muscle, liver, and fat, coupled with increased endogenous glucose production by the liver.⁴ Several popular classes of oral diabetes therapies on the market (e.g., sulfonylureas and PPAR- γ agonists) lower glucose by increasing glucose metabolism either via enhanced insulin secretion or improved insulin sensitivity. The only drug

[†] Metabasis Therapeutics.

[‡] Present address: Biogen Idec, 5200 Research Place, San Diego, CA 92122.

[§] Present address: Genomic Institute of the Novartis Research Foundation, 10715 John Jay Hopkins Drive, San Diego, CA 92121.

^{||} Harvard University.

(1) (a) Wild, S.; Roglic, G.; Green, A.; Sicree, R.; King, H. *Diabetes Care* **2004**, *27*, 1047–1053. (b) DeFronzo, R. A. *Med. Clin. North Am.* **2004**, *88*, 787–835.

(2) Moller, D. E. *Nature* **2001**, *414*, 821–827.

(3) Saydah, S. H.; Fradkin, J. J.; Cowie, C. C. *J. Am. Med. Assoc.* **2004**, *291*, 335–342.

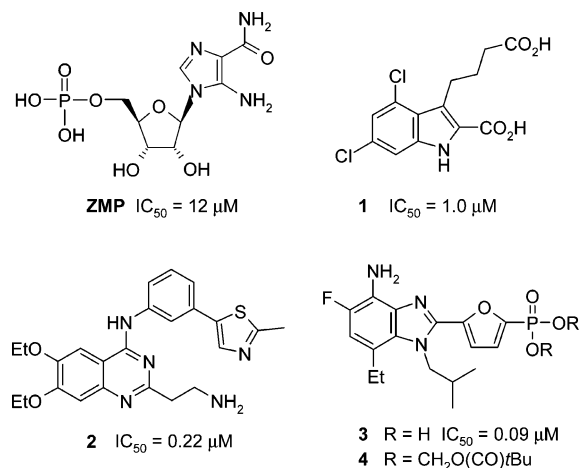
(4) For articles correlating increased endogenous glucose production and elevated glucose levels, see (a) DeFronzo, R. A. *Diabetes* **1988**, *37*, 667–687. (b) Kolterman, O. G.; Gray, R. S.; Griffin, J.; Burstein, P.; Insel, J.; Scarlett, J. A.; Olefsky, J. M. *J. Clin. Invest.* **1981**, *68*, 957–969. (c) Jeng, C. Y.; Sheu, W. H.; Fuh, M. M.; Chen, Y. D.; Reaven, G. M. *Diabetes* **1994**, *43*, 1440–1444. (d) Maggs, D. G.; Buchanan, T. A.; Burant, C. F.; Cline, G.; Gumbiner, B.; Hsueh, W. A.; Inzucchi, S.; Kelley, D.; Nolan, J.; Olefsky, J. M.; Polonsky, K. S.; Silver, D.; Valiquett, T. R.; Shulman, G. I. *Ann. Intern. Med.* **1998**, *128*, 176–185.

that acts primarily by reducing endogenous glucose production is metformin.⁵ Metformin lowers glucose in the absence of weight gain and therefore is often used to treat T2DM despite well-recognized safety concerns associated with its use in certain diabetic patient populations and its overall high incidence of gastrointestinal intolerance.⁶

In an effort to find more effective glucose-lowering drugs, numerous investigators have evaluated various drug targets within the liver for their potential to reduce endogenous glucose production.⁷ Most of the work has focused on enzymes in the gluconeogenesis (GNG) pathway,⁸ since this pathway is responsible for the excessive glucose production found in T2DM.⁹ Phosphoenolpyruvate carboxykinase (PEPCK)¹⁰ and glucose 6-phosphatase (G6Pase)¹¹ were the primary targets in the 1970s and 1980s. In contrast, we targeted fructose-1,6-bisphosphatase (FBPase),¹² an enzyme whose expression is regulated by the hormones insulin and glucagon and whose activity is endogenously inhibited by fructose-2,6-bisphosphate and AMP through their interactions with the substrate and allosteric binding sites, respectively. FBPase is an attractive target not only because it is a rate-controlling enzyme within the GNG pathway but also because it functions only within the GNG pathway, unlike both PEPCK and G6Pase.^{8c} Moreover, adults who are genetically deficient in FBPase activity exhibit relatively normal clinical profiles provided they control their diet and avoid prolonged fasting.¹³

Previous attempts to discover inhibitors of FBPase failed to identify suitable drug candidates (Chart 1). In the 1970s, substrate analogs were evaluated and found to exhibit low inhibitory activity.¹⁴ A nucleoside analog, 5-aminoimidazole-4-carboxamide riboside, was shown in the 1990s to lower glucose after conversion to the corresponding 5'-monophosphate (ZMP) and binding to the allosteric AMP binding site.¹⁵ This compound, however, proved to be a weak, nonspecific AMP

Chart 1. Known FBPase Inhibitors



mimic that could not be significantly improved through synthesis of structural analogs. More recently, efforts were made to identify lead compounds by screening large compound libraries.¹⁶ Noncompetitive inhibitors binding at or near the AMP site^{16a-c} (e.g., **1**) and uncompetitive inhibitors (e.g., **2**) binding at a site with unknown physiologic function near the subunit interface^{16d-f} were identified. All showed only modest inhibitory potency with no reports of glucose lowering activity in animal models.

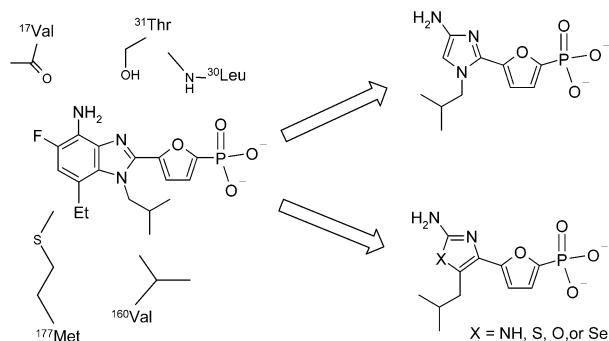
Our strategy was to target the allosteric AMP binding site, which is considerably less hydrophilic than the substrate binding site and completely insensitive to inhibitor-induced FBPase precursor buildup. As outlined in the previous report,¹⁷ AMP binding sites are traditionally difficult drug targets due to their high dependence on electrostatic binding interactions and their common use by enzymes within important anabolic and catabolic pathways. Using a structure-guided drug design strategy, we identified a lead compound (**3**) and showed that it is a potent and specific FBPase inhibitor capable of entering rat hepatocytes.¹⁷

Herein, we describe our efforts to find an orally bioavailable FBPase inhibitor that lowers glucose in diabetic animal models. Since **3** exhibited poor oral activity and known phosphonate prodrugs of **3** (e.g., **4**) failed to achieve adequate oral bioavailability, we re-examined the structure of the FBPase–**3** complex with the goal of identifying a new inhibitor series with properties more likely to produce orally bioavailable compounds. This led to compounds with reduced molecular weight, increased potency, increased solubility, and decreased protein binding. These findings coupled with the identification of a phosphonate

- (5) (a) Stumvoll, M.; Nurjhan, N.; Perriello, G.; Dailey, G.; Gerich, J. E. *N. Engl. J. Med.* **1995**, *333*, 550–554. (b) DeFronzo, R. A.; Goodman, A. M. *N. Engl. J. Med.* **1995**, *333*, 541–549. (c) Hundal, R. S.; Krssak, M.; Dufour, S.; Laurent, D.; Lebon, V.; Chandramouli, V.; Inzucchi, S. E.; Schumann, W. C.; Petersen, K. F.; Landau, B. R.; Shulman, G. I. *Diabetes* **2000**, *49*, 2063–2069. (d) Natali, A.; Ferrannini, E. *Diabetologia* **2006**, *49*, 434–441.
- (6) For reviews see: (a) Howlett, H. C.; Bailey, C. J. *Drug Saf.* **1999**, *20*, 489–503. (b) Dunn, C. J.; Peters, D. H. *Drugs* **1995**, *49*, 721–749.
- (7) For reviews, see: (a) McCormack, J. G.; Westergaard, N.; Kristiansen, M.; Brand, C. L.; Lau, J. *Curr. Pharm. Des.* **2001**, *7*, 1451–1474. (b) Barf, T. *Mini Rev. Med. Chem.* **2004**, *4*, 897–908. (c) Kurukulasuriya, R.; Link, J. T.; Madar, D. J.; Pei, Z.; Richards, S. J.; Rohde, J. J.; Souers, A. J.; Szczepankiewicz, B. G. *Curr. Med. Chem.* **2003**, *10*, 123–153.
- (8) For reviews on the gluconeogenesis pathway and its regulation, see: (a) Pilkis, S. J.; Granner, D. K. *Annu. Rev. Physiol.* **1992**, *54*, 885–909. (b) Granner, D.; Pilkis, S. J. *Biol. Chem.* **1990**, *265*, 10173–10176. (c) In addition to their roles in GNG, PEPCK is also important for cellular energy homeostasis and the red-ox state while G6Pase participates in the conversion of hepatic glycogen to glucose.
- (9) (a) Magnusson, I.; Rothman, D. L.; Katz, L. D.; Shulman, R. G.; Shulman, G. I. *J. Clin. Invest.* **1992**, *90*, 1323–1327. (b) Gastaldelli, A.; Baldi, S.; Pettiti, M.; Toschi, E.; Camastra, S.; Natali, A.; Landau, B. R.; Ferrannini, E. *Diabetes* **2000**, *49*, 1367–1373. (c) Wajngot, A.; Chandramouli, V.; Schumann, W. C.; Ekberg, K.; Jones, P. K.; Efendic, S.; Landau, B. R. *Metabolism* **2001**, *50*, 47–52.
- (10) Newgard, C. B.; Moore, S. V.; Foster, D. W.; McGarry, J. D. *J. Biol. Chem.* **1984**, *259*, 6958–6963.
- (11) Herling, A. W.; Burger, H. J.; Schwab, D.; Hemmerle, H.; Below, P.; Schubert, G. *Am. J. Physiol.* **1998**, *274* (6 Pt 1), G1087–G1093.
- (12) Benkovic, S. J.; deMaine, M. M. *Adv. Enzymol. Relat. Areas Mol. Biol.* **1982**, *53*, 45–82.
- (13) Gitzelmann, R.; Steinmann, B.; Van den Berghe, G. *The Metabolic and Molecular Basis of Inherited Disease*; Scriver, C. R., Beaudet, A. L., Sly, W. S., Valle, D., Eds.; McGraw Hill: New York, 1995; Vol. 1, pp 905–934.
- (14) Pilkis, S. J.; McGrane, M. M.; Kountz, P. D.; el-Maghrabi, M. R.; Pilkis, J.; Maryanoff, B. E.; Reitz, A. B.; Benkovic, S. J. *Biochem. Biophys. Res. Commun.* **1986**, *138*, 159–166.

- (15) (a) Vincent, M. F.; Marangos, P. J.; Gruber, H. E.; Van den Berghe, G. *Diabetes* **1991**, *40*, 1259–1266. (b) Vincent, M. F.; Erion, M. D.; Gruber, H. E.; Van den Berghe, G. *Diabetologia* **1996**, *39*, 1148–1155.
- (16) (a) Wright, S. W.; Carlo, A. A.; Danley, D. E.; Hageman, D. L.; Karam, G. A.; Mansour, M. N.; McClure, L. D.; Pandit, J.; Schulte, G. K.; Treadway, J. L.; Wang, I. K.; Bauer, P. H. *Bioorg. Med. Chem. Lett.* **2003**, *13*, 2055–2058. (b) von Geldern, T. W.; Lai, C.; Gum, R. J.; Daly, M.; Sun, C.; Fry, E. H.; Abad-Zapatero, C. *Bioorg. Med. Chem. Lett.* **2006**, *16*, 1811–1815. (c) Lai, C.; Gum, R. J.; Daly, M.; Fry, E. H.; Hutchins, C.; Abad-Zapatero, C.; von Geldern, T. W. *Bioorg. Med. Chem. Lett.* **2006**, *16*, 1807–1810. (d) Wright, S. W.; et al. *J. Med. Chem.* **2002**, *45*, 3865–3877. (e) Wright, S. W.; Hageman, D. L.; McClure, L. D.; Carlo, A. A.; Treadway, J. L.; Mathiowetz, A. M.; Withka, J. M.; Bauer, P. H. *Bioorg. Med. Chem. Lett.* **2001**, *11*, 17–21. (f) Choe, J. Y.; Nelson, S. W.; Arienti, K. L.; Axe, F. U.; Collins, T. L.; Jones, T. K.; Kimmich, R. D.; Newman, M. J.; Norvell, K.; Ripka, W. C.; Romano, S. J.; Short, K. M.; Slee, D. H.; Fromm, H. J.; Honzatko, R. B. *J. Biol. Chem.* **2003**, *278*, 51176–51183.
- (17) Erion, M. D.; Dang, Q.; Reddy, M. R.; Kasibhatla, S. R.; Huang, J.; Lipscomb, W. N.; van Poelje, P. D. *J. Am. Chem. Soc.* **2007**, *129*, 15480–15490.

Scheme 1. Drug Design Strategy



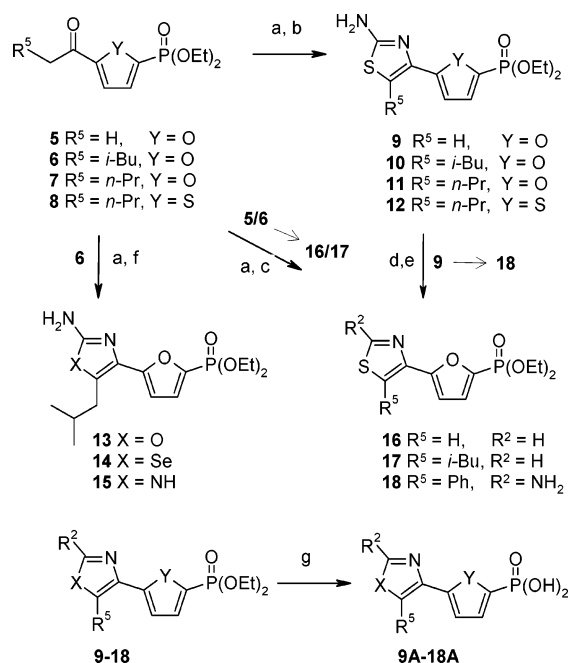
prodrug strategy that enables good oral bioavailability led to the discovery of MB06322 (CS-917), a compound that markedly lowers glucose levels in animals^{18,19} and in humans.²⁰

Results

Inhibitor Design. The initial lead inhibitor, **3**, lowered glucose levels in fasted normal rats and in several diabetic animal models after systemic administration (data not shown) but failed to lower glucose after oral administration (≤ 100 mg/kg) due to low oral bioavailability ($\sim 1\%$). Standard phosphonate prodrugs²¹ of **3**, such as the bispivaloyloxymethyl prodrug **4**, increased the oral bioavailability ($\sim 2.4\%$), but not to acceptable levels. Low oral bioavailability was attributed to a variety of structural features commonly associated with low absorption,²² including high molecular weight (~ 610), low solubility (< 10 $\mu\text{g/mL}$), as well as aqueous and metabolic instability. Consequently, major changes to either the inhibitor structure and/or the prodrug strategy appeared necessary to achieve the desired oral bioavailability.

Efforts to redesign the inhibitor focused on structural modifications that retained the binding interactions shown previously to contribute significantly to the overall binding affinity, i.e., hydrogen bonds with the phosphonate, amino group, and imidazole nitrogen.¹⁷ Since the 6-membered ring in the benzimidazole base contributed little to the overall binding affinity¹⁷ while adding significantly to the molecular weight and poor aqueous solubility, we modeled compounds in which the benzimidazole was replaced with five- and six-membered heterocyclic compounds containing an amino group and a furanylphosphonate (Scheme 1). Importantly these studies showed that the distance between the amino and PO_3^{2-} groups was still within the range required to simultaneously interact with the phosphate and purine binding sites (4.0–5.5 Å). Low energy conformations also showed that hydrogen bonds between the amino group and FBPase residues V17 and T31 were possible as were favorable interactions with the imidazole nitrogen and furanyl oxygen.

One potential limitation in the design strategy that required attention early on was the well-recognized instability of electron-rich azoles, including amino substituted pyrroles and both 4-

Scheme 2^a

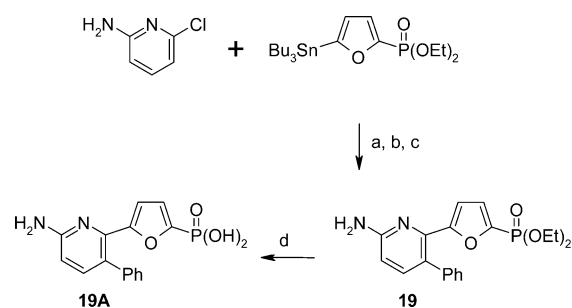
^a Conditions: (a) CuBr_2 , EtOH; (b) thiourea, EtOH; (c) formamide, P_4S_{10} , benzene; (d) NBS, CHCl_3 ; (e) PhB(OH)_2 , $\text{Pd(PPh}_3)_4$, DME-EtOH, NaHCO_3 , 80°C ; (f) urea (for oxazole **13**), or selenourea (for selenazole **14**) or guanidine-HCl (for imidazole **15**), *t*-BuOH, 80°C ; (g) TMSBr, CH_2Cl_2 .

and 5-aminoimidazoles.²³ Alternatively, 2-aminoimidazoles were reported to exhibit good stability²⁴ and based on modeling studies were expected to form the same binding site interactions if the furanylphosphonate and alkyl substituents were attached at the 4- and 5-positions, respectively (Scheme 1).

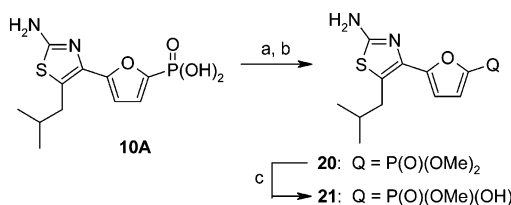
Synthesis of FBPase Inhibitors. Five-membered heterocyclic phosphonates were synthesized from readily accessible 2-acylfuran-5-phosphonate diesters as outlined in Scheme 2. The thiazole analogs **9–12** were prepared from compounds **5–8** by α -bromination followed by cyclization with thiourea. Reaction of the α -bromide of **6** with urea, selenourea, and guanidine gave oxazole (**13**), selenazole (**14**), and imidazole (**15**) phosphonate diesters, respectively. The 2-desamino analogs **16** and **17** were prepared from compounds **5** and **6**, respectively, by α -bromination followed by cyclization with in situ generation of thioformamide. The C5 phenyl thiazole analog **18** was prepared from **9** via bromination followed by a Suzuki coupling with phenyl boronic acid. The pyridine phosphonate diester **19** was synthesized using a Stille coupling of 5-diethylphosphono-2-tributylstannylfuran and 2-amino-6-chloropyridine followed by bromination of the 2-aminopyridine and a Suzuki coupling with phenyl boronic acid (Scheme 3). Conversion of the phosphonate diethyl esters (**9–19**) to the corresponding phosphonic acids (**9A–19A**) was accomplished using TMSBr. The dimethyl ester **20** was prepared from **10A** by treating the corresponding phosphonodichloridate with methanol in the presence of diiso-

- (18) Erion, M. D.; van Poelje, P. D.; Dang, Q.; Kasibhatla, S. R.; Potter, S. C.; Reddy, M. R.; Reddy, K. R.; Jiang, T.; Lipscomb, W. N. *Proc. Natl. Acad. Sci. U.S.A.* **2005**, *102*, 7970–7975.
 (19) van Poelje, P. D.; Potter, S. C.; Chandramouli, V. C.; Landau, B. R.; Dang, Q.; Erion, M. D. *Diabetes* **2006**, *55*, 1747–1754.
 (20) Triscari, J.; Walker, J.; Feins, K.; Tao, B.; Bruce, S. R. *Diabetes* **2006**, *55* (Suppl 1), 444P.
 (21) Krise, J. P.; Stella, V. J. *Adv. Drug Delivery Rev.* **1996**, *19*, 287–310.
 (22) Lipinski, C. A.; Lombardo, F.; Dominy, B. W.; Feeney, P. J. *Adv. Drug Delivery Rev.* **1997**, *23*, 3–25.

- (23) (a) Lawson, A. *J. Chem. Soc.* **1956**, 307–310. (b) McLaughlin, M.; Mohareb, R. M.; Rapoport, H. *J. Org. Chem.* **2002**, *68*, 50–54. (c) Dang, Q.; Liu, Y.; Erion, M. D. *J. Am. Chem. Soc.* **1999**, *121*, 5833–5834.
 (24) No instability has been reported on the numerous natural products that contain a 2-aminoimidazole moiety. For example, (a) Bromoageliferin, Huigens, III, R. W.; Richards, J. J.; Parise, G.; Ballard, T. E.; Zeng, W.; Deora, R.; Melander, C. *J. Am. Chem. Soc.* **2007**, *129*, 6966–6967. (b) Mauritiamine, Tsukamoto, S.; Kato, H.; Hirota, H.; Fusetani, N. *J. Nat. Prod.* **1996**, *59*, 501–503. (c) Zoanthoxanthins, Xu, Y.; Yakushijin, K.; Horne, D. A. *Tetrahedron Lett.* **1999**, *33*, 4385–4388.

Scheme 3^a

^a Conditions: (a) Pd(PPh₃)₄, *p*-xylene, 170 °C; (b) Br₂, AcOH; (c) Ph-B(OH)₂, Pd(PPh₃)₄, DME-EtOH, NaHCO₃, 80 °C; (d) TMSBr, CH₂Cl₂.

Scheme 4^a

^a Conditions: (a) SOCl₂, pyridine, (CH₂Cl)₂; (b) MeOH, *i*-Pr₂NEt; (c) NaOH.

Table 1. FBPase Inhibitor Structure–Activity Relationships

cpmd	X	Y	Q	R ²	R ⁵	HL IC ₅₀ (nM) ^a	RL IC ₅₀ (nM) ^b
AMP	–	–	–	–	–	1000	20 000
ZMP	–	–	–	–	–	12 000	310 000
3	–	–	–	–	–	90	370
9A	S	O	PO ₃ H ₂	NH ₂	H	450	13 000
10A	S	O	PO ₃ H ₂	NH ₂	<i>i</i> Bu	16	61
11A	S	O	PO ₃ H ₂	NH ₂	<i>n</i> Pr	30	ND ^c
12A	S	S	PO ₃ H ₂	NH ₂	<i>n</i> Pr	>10 000 ^d	ND
13A	O	O	PO ₃ H ₂	NH ₂	<i>i</i> Bu	120	2000
14A	Se	O	PO ₃ H ₂	NH ₂	<i>i</i> Bu	39	150
15A	NH	O	PO ₃ H ₂	NH ₂	<i>i</i> Bu	5000	ND
16A	S	O	PO ₃ H ₂	H	H	5500	ND
17A	S	O	PO ₃ H ₂	H	<i>i</i> Bu	500	3500
18A	S	O	PO ₃ H ₂	NH ₂	Ph	14	500
19A	CH=CH	O	PO ₃ H ₂	NH ₂	Ph	42	1600
20	S	O	PO(OMe) ₂	NH ₂	<i>i</i> Bu	>10 000 ^e	ND
21	S	O	PO(OH)(OMe)	NH ₂	<i>i</i> Bu	>10 000 ^f	ND
22	S	O	CO ₂ H	NH ₂	Ph	>10 000	ND

^a Inhibition of human liver FBPase. ^b Inhibition of rat liver FBPase. ^c ND denotes not determined. ^d Thirty percent at 10 μM. ^e Greater than 3 mM. ^f Greater than 400 μM.

propylethylamine (Scheme 4). Hydrolysis of **20** with NaOH gave the monomethyl ester **21**.

FBPase Inhibitor Structure–Activity Relationships. Synthesis and evaluation of substituted 5- and 6-membered heterocyclic bases attached to the 5-position of 2-phosphonfuran led to the discovery of a new class of potent FBPase inhibitors (Table 1). The imidazole analog (**15A**) showed modest inhibitor potency (IC₅₀ = 5 μM, Table 1), suggesting that most of the binding interactions observed in the benzimidazole series (e.g., **3**)¹⁷ were likely retained despite removal of one aryl ring, the translocation of the amino group to the 5-membered heterocycle, and the rearrangement of the heterocycle nitrogen atoms. Replacement of the imidazole with a thiazole (**10A**, IC₅₀ = 16

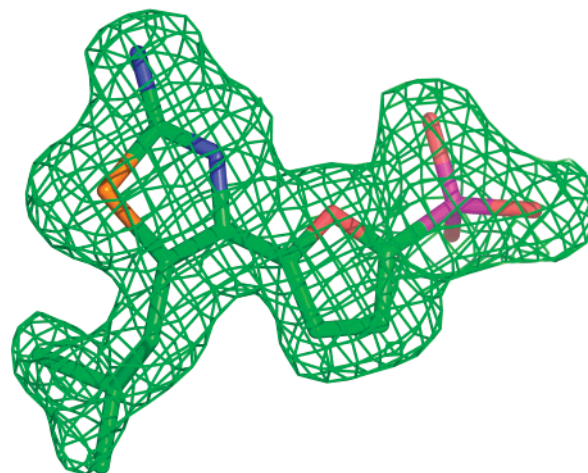


Figure 1. The 2F_o–F_c electron density map is contoured at 1 σ and superimposed on the refined model of the human FBPase–**10A** complex at 2.0 Å resolution.

nM) led to a 312-fold improvement in inhibitory potency and correspondingly to a compound 63- and 5.6-fold more potent than AMP and **3**, respectively.

Evidence that **10A** interacts with the binding site using many of the same interactions predicted by the initial molecular modeling studies was indirectly derived from the inhibitory potencies of closely related analogs (Table 1). Favorable hydrogen bond interactions by the 2-amino group and van der Waals interactions by the 5-*i*-butyl group were suggested by the 28- and 31-fold reduction in inhibitory potencies observed for the corresponding **10A** analogs, **17A** and **9A**, respectively, as well as by the additive loss of inhibitory potency found for the analog (**16A**) that contains neither group. Replacement of the furan with a thiophene (**12A**) led to a 344-fold decrease in potency indicating that like **3**, **10A** likely forms a weak but favorable electrostatic interaction between the furanyl oxygen and the amido hydrogen of L30. Consistent with previous series,¹⁷ the phosphonate proved to be essential for binding as evidenced by the inability of the dimethylester **20**, the monomethyl ester **21**, or the corresponding carboxylate (**22**) to inhibit FBPase.

Less apparent from analysis of the binding interactions was the dependence of the inhibitory potency on the heterocyclic base. Replacement of N1 in the imidazole analog (**15A**) with sulfur (**10A**), selenium (**14A**), and oxygen (**13A**) led to a 312-, 128-, and 42-fold improvement in potency, respectively. Analogously, replacement of the nitrogen with –CH=CH– and the alkyl group with phenyl produced a compound (**19A**) with a six-membered heterocycle (pyridyl) and good inhibitory potency (IC₅₀ = 42 nM).

Enzyme Specificity. The lead inhibitor **10A** exhibited high specificity for the AMP binding site of FBPase based on its lack of activity against five AMP binding enzymes, namely human erythrocyte AMP deaminase, rabbit muscle glycogen phosphorylase, human AMP-activated protein kinase, rabbit muscle adenylate kinase, and rabbit liver phosphofructokinase.¹⁸

X-Ray Crystallography. The three-dimensional structure of the human FBPase–**10A** inhibitor complex was solved at 2.0 Å resolution (Figure 1, Table 2). The structure showed that **10A** binds to the AMP binding site and forms the predicted interactions with the binding site residues (Figure 2, Table 3).

Table 2. Data Processing and Refinement Statistics^a

	FBPase-10A
space group	$P2_12_12_1$
cell dimensions	$a = 67.9 \text{ \AA}$, $b = 84.2 \text{ \AA}$, $c = 280.7 \text{ \AA}$
data collection and processing	
wavelength (Å)	0.9764
resolution (Å)	2.0 (2.07–2.00)
reflections	464 199 (5,598)
unique reflections	100 278
completeness (%)	91.5 (51.8)
multiplicity	4.6 (1.6)
R_{sym}^b (%)	17.0 (37.5)
mean I/σ	7.2 (1.3)
number of molecules in asymmetric unit	4
refinement statistics	
R_{working}^c	20.4 (31.9)
R_{free}^d	24.4 (32.9)
average B -factor (Å ²)	21.0
R.M.S. bond (Å)	0.0055
R.M.S. angle (deg)	1.24
number of protein atoms	9858
number of water molecules	1020

^a Values in the parentheses apply to the outer resolution shell. ^b $R_{\text{sym}} = \sum_{hkl} \sum_i |I_i(hkl) - \langle I(hkl) \rangle| / \sum_{hkl} \sum_i I_i(hkl)$, where $I_i(hkl)$ is the intensity of an individual reflection, and $\langle I(hkl) \rangle$ is the mean intensity obtained from the multiple observations of symmetry-related reflections taken from one crystal. ^c $R_{\text{working}} = \sum_{hkl} (|F_o(hkl) - F_c(hkl)|) / \sum_{hkl} (|F_o(hkl)|)$, calculated from reflections in the working set. ^d $R_{\text{free}} = \sum_{hkl} (|F_o(hkl) - F_c(hkl)|) / \sum_{hkl} (|F_o(hkl)|)$, calculated from reflections in the test set, which is a random 5% data set selected from the whole data set.

As depicted by modeling studies conducted in advance of both the synthesis and the X-ray structure, **10A** forms a full complement of interactions with the phosphate binding site. In addition, the amino group formed hydrogen bonds with the side chain hydroxyl of T31 and the backbone carbonyl of V17 whereas the thiazole nitrogen formed a favorable electrostatic interaction with T31. Furthermore, the C5 *i*-butyl group resided within van der Waals contact of a hydrophobic surface formed by the sidechains of M177, L30, and V160.

Free-Energy Calculations. A series of *post hoc* free-energy perturbation (FEP) calculations²⁵ provided additional insight into the binding site interactions of the lead inhibitor series as well as other factors that contribute to the observed inhibitory potencies.²⁶ Calculations comparing close structural analogs were performed using a single topology and a total of 479 ps of molecular dynamics (MD) simulation whereas calculations comparing analogs with more substantial structural changes were performed using the thread method²⁷ and a total of 938 ps of MD simulation (see Methods). The results from the FEP calculations using the FBPase model²⁸ (Table 4) were consistent with the experimental findings in that the binding affinity for the imidazole analog (**15A**), regardless of the NH tautomer evaluated, was at least 2.8 kcal/mol weaker relative to the corresponding thiazole analog, **10A**. The oxazole was intermediate in its inhibitory potency (**10A** → **13A**, $\Delta\Delta G_{\text{bind}} = 1.7 \pm 0.7$ kcal/mol), which was also consistent with the experimental

finding. Analysis of the relative differences in solvation free energies ($\Delta\Delta G_{\text{sol}} = \Delta G_{\text{aq}} - \Delta G_{\text{gas}}$) suggested that the main reason for the differences in potency relate to the energy costs required to desolvate the heterocycle with the imidazole and oxazole requiring 1.5 and 1.2 kcal/mol more to desolvate than the thiazole, respectively. In addition, the transformation of the *i*-butyl thiazole to a phenyl-substituted pyridine (**10A** → **19A**) using the thread method gave a calculated result (1.5 ± 1.2 kcal/mol) consistent with the experimental finding (2.0 kcal/mol).

FEP calculations were also conducted to evaluate the contribution of various binding site interactions, including those by the furanyl oxygen, 2-amino group, and 5-alkyl group (Table 4). The thiazole analog with a thiophene spacer (**12A**) exhibited reduced binding affinity (2.7 ± 0.7 kcal/mol) relative to the furan spacer due to decreased enthalpic energy, which was partially offset by its reduced desolvation energy (3.4 kcal/mol, **10A** → **12A**). Consistent with the experimental findings, removal of the 2-amino group, the alkyl side chain, or both led to significantly reduced binding affinities of 1.7, 1.5, and 3.1 kcal/mol, respectively, confirming the importance of the binding interactions made by these groups with the AMP binding site.

Phosphonic Diamides. The oral bioavailability of **10A** was less than 4% in rats presumably due to its high negative charge at physiological pH. Standard phosphonate prodrugs²¹ such as the acyloxyalkyl²⁹ (**23**), *p*-acetoxybenzyl³⁰ (**24**), *S*-acyl-2-thioethyl³¹ (**25**), and phenyl³² (**26**) esters generally led to some improvement (Table 5) but not to oral bioavailabilities above 15%. Modest oral bioavailability was also observed with prodrugs (e.g., **27**) that cleave following a cytochrome P450 3A-catalyzed oxidation of the ring methine.³³ As part of these efforts, we also explored the potential of phosphonic amides as prodrugs. Aryl phosphonamidates were prepared based on cell studies with nucleoside monophosphates,³⁴ which showed that the intermediate mono-amide generated after esterase-catalyzed cleavage of the carboxylic ester and subsequent expulsion of phenol, was converted to the diacid via a phosphoramidase-catalyzed cleavage of the P–N bond.³⁵ The corresponding prodrug of **10A**, **28**, exhibited moderate aqueous instability (pH = 7.0, $t_{90} = 14$ h), rapid esterase-catalyzed conversion to the

- (25) (a) Zwanzig, R. J. *J. Chem. Phys.* **1954**, *22*, 1420–1426. (b) Tembe, B. L.; McCammon, J. A. *Comput. Chem.* **1984**, *8*, 281–283. (c) Kollman, P. A. *Chem. Rev.* **1993**, *93*, 2395–2417.
(26) For reviews of FEP calculations in drug design and lead optimization, see: (a) Jorgensen, W. L. *Science* **2004**, *303*, 1813–1818. (b) *Free Energy Calculations in Rational Drug Design*; Reddy, M. R., Erion, M. D., Eds.; Kluwer/Plenum Press: New York, 2001.
(27) Singh, U. C.; Benkovic, S. J. *Proc. Natl. Acad. Sci. U.S.A.* **1988**, *85*, 9518–9523.

- (28) (a) Reddy, M. R.; Erion, M. D. *J. Am. Chem. Soc.* **2001**, *123*, 6246–6252. (b) Erion, M. D.; van Poelje, P. D.; Reddy, M. R. *J. Am. Chem. Soc.* **2000**, *122*, 6114–6215. (c) Reddy, M. R.; Erion, M. D.; Agarwal, A. In *Reviews in Computational Chemistry*; Lipkowitz, K. B., Boyd, D. B., Eds.; Wiley-VCH Inc.: New York, 2000; Vol. 16, pp 217–304.
(29) Farquhar, D. S.; D. N.; Katesch, N. J.; Saunders, P. P. *J. Pharm. Sci.* **1983**, *72*, 324–325.
(30) (a) Mitchell, A. G.; Thompson, W.; Nicholls, D.; Irwin, W. J.; Freeman, S. J. *Chem. Soc. Perkins Trans. I* **1992**, 2345–2353. (b) Dang, Q.; Liu, Y.; Rydzewski, R. M.; Brown, B. S.; Robinson, E.; van Poelje, P. D.; Colby, T. J.; Erion, M. D. *Bioorg. Med. Chem. Lett.* **2007**, *17*, 3412–3416.
(31) Peyrottes, S.; Egron, D.; Lefebvre, I.; Gosselin, G.; Imbach, J. L.; Perigaud, C. *Mini Rev. Med. Chem.* **2004**, *4*, 395–408.
(32) De Lombaert, S.; Erion, M. D.; Tan, J.; Blanchard, L.; el-Chehab, L.; Ghai, R. D.; Sakane, Y.; Berry, C.; Trapani, A. J. *J. Med. Chem.* **1994**, *37*, 498–511.
(33) Erion, M. D.; Reddy, K. R.; Boyer, S. H.; Matelich, M. C.; Gomez-Galeno, J.; Lemus, R. H.; Ugarkar, B. G.; Colby, T. J.; Schanzer, J.; van Poelje, P. D. *J. Am. Chem. Soc.* **2004**, *126*, 5154–5163.
(34) (a) McGuigan, C.; Pathirana, R. N.; Balzarini, J.; De Clercq, E. *J. Med. Chem.* **1993**, *36*, 1048–1052. (b) Perrone, P.; Luoni, G. M.; Kelleher, M. R.; Daverio, F.; Angell, A.; Mulready, S.; Congiatu, C.; Rajyaguru, S.; Martin, J. A.; Leveque, V.; Le Pogam, S.; Najera, I.; Klumpp, K.; Smith, D. B.; McGuigan, C. *J. Med. Chem.* **2007**, *50*, 1840–1849. (c) McGuigan, C.; Pathirana, R. N.; Mahmood, N.; Devine, K. G.; Hay, A. J. *Antiviral Res.* **1992**, 311–321.
(35) Sabouard, D.; Naesens, L.; Cahard, D.; Salgado, A.; Pathirana, R.; Velazquez, S.; McGuigan, C.; De Clercq, E.; Balzarini, J. *Mol. Pharmacol.* **1999**, *56*, 693–704.

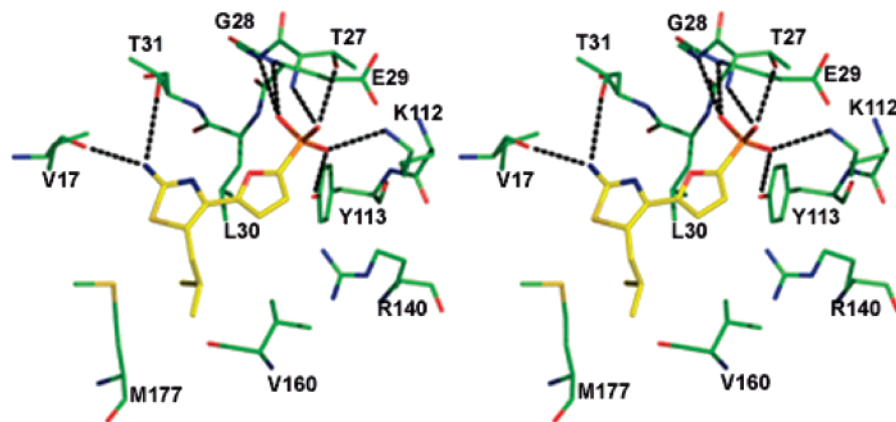


Figure 2. Stereodiagram derived from the X-ray structure of the human FBPase–10A. Putative hydrogen bonds are shown as dotted lines when the distance between the hydrogen bond acceptor and donor is less than 3.3 Å.

Table 3. Binding Site Interaction Distances

hydrogen bond		FBPase–AMP	FBPase–10A	
AMP/10A	residue	X-ray ^a	Model ^b	X-ray ^c
NH ₂	O=C (V17)	2.98	3.08	3.05
NH ₂	HO (T31)	3.23	2.89	3.00
N	HO (T31)	3.54	3.46	4.08
O (furanyl)	HN (L30)	NA	4.59	4.38
⁵ O (ribose)	HO (Y113)	2.98	–	–
³ O (ribose)	HO (Y113)	2.53	–	–
³ O (ribose)	HNξ (R140)	2.95	–	–
OP	HN (E29)	2.78	2.79	2.76
OP	HN (G28)	2.89	2.89	3.30
OP	HO (T27)	2.73	3.18	3.03
OP	HN (T27)	2.88	3.01	2.53
OP	HNε (K112)	2.91	2.78	2.62
OP	HO (Y113)	2.70	2.56	2.69
OP	HN (L30)	3.19	–	–
	base to P distance	4.24	5.28	5.19
	NH ₂ to P distance	7.27	7.40	7.31

^a Distances in angstroms for X-ray structure of human FBPase–AMP complex; NA = not applicable. ^b Distances in angstroms for computer model of human FBPase–10A complex. ^c Distances in angstroms for X-ray structure of human FBPase–10A complex (2.0 Å resolution).

phosphonamidic acid and low oral bioavailability (Table 5). Remarkably, the diamides **29–31** displayed good aqueous stability (pH = 7.0, *t*₉₀ > 2 days) and, in general, were converted much more slowly to the phosphonamidic acid by esterases. Most importantly, the diamides **29–31** exhibited significantly better oral bioavailabilities (22–47%) than the other phosphonamide prodrug classes (Table 5).

Diamide Prodrug Synthesis. Prodrugs **23–28** were prepared using methods previously described in the literature (see Supporting Information). Diamide phosphonate prodrugs **29–31** were prepared by converting **10A** to its corresponding dichloridate using thionyl chloride and pyridine followed by condensation with the corresponding amino acid ester (Scheme 5).

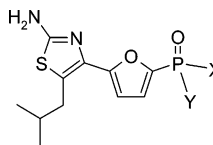
Diamide Prodrug Cleavage Mechanism. Although the cleavage mechanism was assumed to be similar to that reported for the monoamidate prodrugs,³⁵ the difference in leaving group (α-amino acid vs phenol) led us to conduct several studies monitoring the production of prodrug cleavage products. Incubation of MB06322 (**30**) with rat hepatocytes (Figure 3) as well as rat liver S9 preparations (data not shown) led to a time-dependent loss of the prodrug and the simultaneous production of **10A** along with an additional product. LC-MS analysis of the prodrug cleavage products suggested that the new product

Table 4. Relative Free Energies

transformation (S1 → S2) ^a		ΔΔG _{sol}	ΔΔG _{bind}	ΔΔG _{bind} (exp)
10A → 13A ^b	S → O	−1.2 ± 0.5	1.7 ± 0.7	1.2
10A → 15A ^b	S → NH (tau1) ^c	−2.3 ± 0.6	3.0 ± 0.7	3.4
10A → 15A ^b	S → N; N → (tau2) ^d	−1.4 ± 0.6	2.8 ± 0.7	3.4
10A → 9A ^e	<i>i</i> Bu → H	−0.9 ± 0.6	1.5 ± 0.7	2.0
10A → 17A ^b	NH ₂ → H	3.6 ± 0.6	1.7 ± 0.7	2.1
10A → 16A ^e	<i>i</i> Bu → H and NH ₂ → H	2.6 ± 0.7	3.1 ± 0.8	3.5
10A → 19A ^e	<i>i</i> Bu → Ph and S → HC=CH	−1.3 ± 1.1	1.5 ± 1.2	0.6
11A → 12A ^b	O → S	1.4 ± 0.5	2.7 ± 0.7	3.4

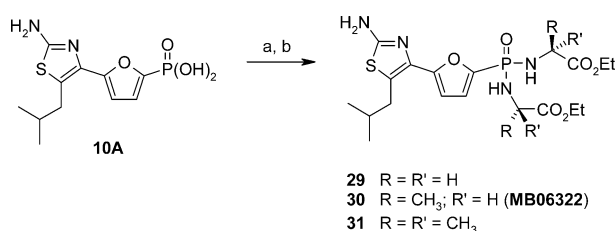
^a Complexes generated from FBPase–10A structure. ^b Single topology. ^c Tautomer 1 (tau1). ^d Tautomer 2 (tau2). ^e Double topology.

was the phosphonamidic acid **33** (Scheme 6), which was subsequently confirmed by comparing the HPLC retention time with an independently synthesized synthetic standard. Incubation of MB06322 with purified pig liver carboxylesterase also led to **33**, but not **10A**, suggesting that a carboxylesterase catalyzed the initial step in the prodrug cleavage mechanism. Intermediate **33** presumably arises from the esterase-cleavage product, **32**, which rapidly proceeds to **33** via a nonenzymatic, unimolecular reaction involving carboxylate-assisted elimination of an amino acid and transient formation of a 5-membered cyclic compound (Scheme 6). **33** was demonstrated to be a prodrug cleavage intermediate based on its conversion to **10A** in the presence of rat liver S9. The conversion rate (0.019 nmoles/min/mg protein) was similar to the rate for prodrug MB06322 suggesting that the second step was the slow step in the production of the phosphonic acid **10A**. The phosphoramidase that catalyzes the latter step was isolated and shown to be distinct from the phosphoramidase³⁵ catalyzing the final step in the conversion of previously reported aryl phosphonamidates based on its molecular weight (20 vs 50–100 kD) and preferred substrates (J. Stebbins, personal communication).³⁶

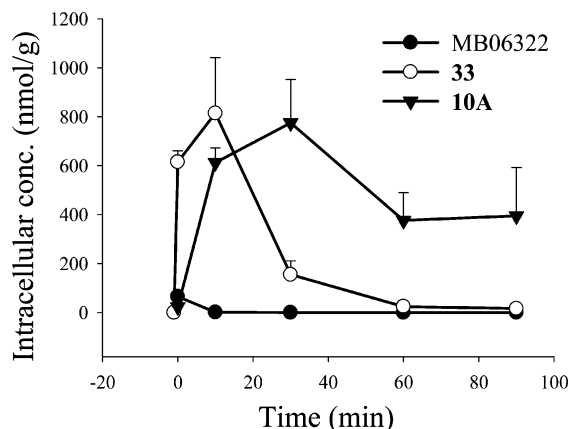
Table 5. FBPase Inhibitor Prodrug SAR^a


cmpd	X	Y	MW	cLogP ^b	t ₉₀ ^c (hours)	ECR ^d (nmole/min/mg)	%F ^e
3	—	—	381.3	3.72	NA	NA	0.9
4	—	—	609.6	6.81	ND	ND	2.4
10A	OH	OH	302.3	1.60	NA	NA	<4
23	O-POM	O-POM	530.6	5.01	<4	>300	11
24	O-PAB	O-PAB	598.6	4.88	<4	>300	8
25	O-SATE	O-SATE	506.6	3.09	8	>300	ND
26	OPh	OPh	454.5	5.24	ND	ND	0.2
27	—OCH(3-Br-Ph)CH ₂ CH ₂ O—		497.4	4.95	ND	ND	11
28	OPh	Ala-OEt	477.5	5.17	14	55	12
29	Gly-OEt	Gly-OEt	472.5	3.65	36	43	26
30	Ala-OEt	Ala-OEt	500.6	4.16	>48	11	22
31	Ala(Me)-OEt	Ala(Me)-OEt	528.6	5.11	>48	8	47

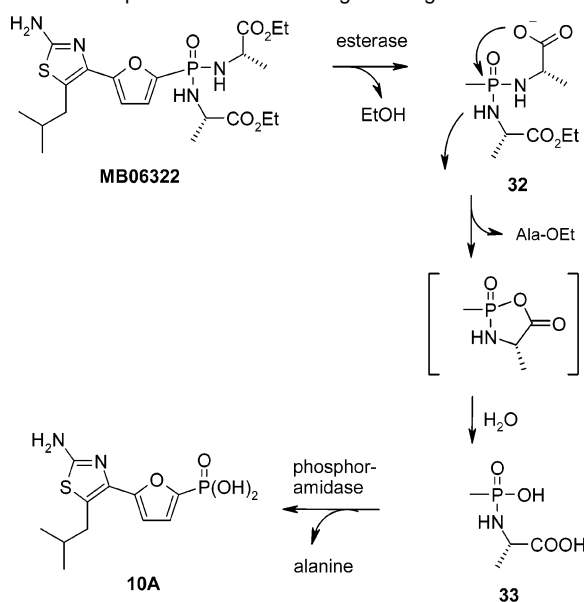
^a Abbreviations: NA, not applicable; ND, not determined; POM, pivaloyloxymethylene; PAB, para-acetoxybenzyl; SATE, S-acyl-2-thioethyl. ^b Calculated using ADME Boxes *v.* 3.5. ^c Prodrug stability at 37 °C in 100 mM potassium phosphate (pH 7) wherein t₉₀ represents the time (in hours) required for 10% loss in the prodrug concentration. ^d ECR, esterase conversion rate for prodrugs incubated with rat liver S9 (2 mg/mL) at 37 °C. ^e Oral bioavailability determined by measuring urinary excretion of **10A** following oral administration of the prodrug vs *i.v.* administration of **10A**.

Scheme 5^a

^a Conditions: (a) SOCl₂, pyridine, (CH₂Cl)₂; (b) glycine ethyl ester or L-alanine ethyl ester or 2-methylalanine ethyl ester, *i*-Pr₂NEt, CH₂Cl₂, 0 °C.

**Figure 3.** Time course for conversion of prodrug MB06322 to **10A** in freshly isolated rat hepatocytes.**Inhibition of Glucose Production from Rat Hepatocytes.**

Concentration-dependent inhibition of the gluconeogenesis pathway was demonstrated in studies measuring glucose production by hepatocytes freshly isolated from fed male Zucker Diabetic Fatty (ZDF) rats (Figure 4A). The inhibitory potency of MB06322 was independent of whether glucose production was from lactate (IC₅₀ = 1.3 ± 0.1 μM) or glycerol (IC₅₀ = 1.2 ± 0.8 μM) and therefore consistent with the expected mechanism, *i.e.*, inhibition of gluconeogenesis via inhibition of FBPase.

Scheme 6. Proposed Diamide Prodrug Cleavage Mechanism

Metformin was also evaluated for its ability to inhibit glucose production by rat hepatocytes based on reports indicating that metformin inhibits gluconeogenesis in humans⁵ and rodents,³⁷ albeit by an indirect mechanism that remains poorly defined.³⁸ Metformin inhibited glucose production from either lactate (IC₅₀ = 2200 ± 300 μM) or glycerol (IC₅₀ = 3400 ± 1200 μM) with a potency >1000-fold less than that of MB06322 (Figure 4A). Moreover, metformin and MB06322 differed in their effect

- (36) The major phosphoramidase activity responsible for hydrolysis of the monoamidate of **10A** was purified to near homogeneity from rat liver. In addition to catalyzing the cleavage of the phosphoramidic acid **33** to the phosphonic acid **10A** and alanine, the enzyme readily cleaved AMP-phosphoramidate to AMP and ammonia. Previously reported aryl phosphoramidates of the 5'-monophosphate of AZT (ref 34c) and PMEA (Keith, K. A.; Hitchcock, M. J. M.; Lee, W. A. Holy, A.; Kern, E. R. *Antimicrob. Agents Chemother.* **2003**, *47*, 2193–2198) were not hydrolyzed by this phosphoramidase preparation. Some conversion may occur by chemical hydrolysis, which is fast at low pH (Lee, W. A.; He, G. X.; Eisenberg, E.; Cihlar, T.; Swaminathan, S.; Mulato, A.; Cundy, K. C. *Antimicrob. Agents Chemother.* **2005**, *49*, 1898–1906).
- (37) Shaw, R. J.; Lamia, K. A.; Vasquez, D.; Koo, S. H.; Bardeesy, N.; Depinho, R. A.; Montminy, M.; Cantley, L. C. *Science* **2005**, 1642–1646.

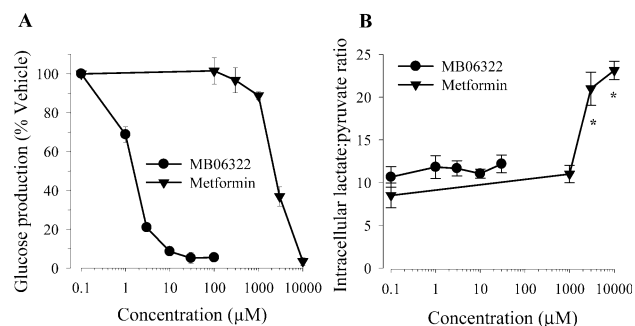


Figure 4. Metabolic effects of MB06322 and metformin in male ZDF rat hepatocytes isolated in the fed state. (A) Inhibition of glucose production from ^{14}C -lactate. (B) Intracellular lactate/pyruvate ratio with 1 mM glycerol as the carbon source. All parameters were assessed in duplicate samples following 30 min of preincubation with drug followed by 1 h of incubation with substrate. Average results from three separate cell preparations are shown. * $p < 0.05$ compared to controls, student's t -test.

on cellular redox potential³⁹ with metformin resulting in an increase in the lactate/pyruvate ratio at concentrations required to inhibit glucose production (Figure 4B). In addition, as expected for an inhibitor of an energy-consuming process, MB06322 treatment resulted in increased energy charge and ATP levels, whereas metformin showed decreased ATP levels and no change in energy charge due to its concomitant effects on the cellular redox potential (Table 6).

In Vivo Activity. Acute administration of MB06322 or metformin to fasting ZDF rats resulted in significant glucose lowering (Figure 5A–B) without evidence of hypoglycemia even at doses 10-fold above the minimum efficacious dose. Glucose lowering was linked to inhibition of gluconeogenesis and endogenous glucose production for MB06322 but not metformin. Gluconeogenesis was evaluated by measuring ^{14}C -glucose following intravenous administration of ^{14}C -bicarbonate to fasted ZDF rats (Figure 5C). MB06322 at doses of 30 and 300 mg/kg inhibited *de novo* glucose synthesis, *ca.* 30 and 85%, respectively, whereas metformin at a dose (1000 mg/kg) that significantly lowered glucose (–155 mg/dL) failed to inhibit the incorporation of ^{14}C -bicarbonate into glucose. Consistent with these findings, MB06322 at the minimum efficacious dose (30 mg/kg) reduced endogenous glucose production to a significantly greater extent than vehicle (–45.3 vs –17.1%, $p < 0.05$) whereas metformin (1000 mg/kg) had no effect (–4.3%, NS) (Figure 5D).

Discussion

Analysis of the FBPase complexes containing AMP,⁴⁰ **3**,¹⁷ and **10A** highlighted the common binding interactions and those unique to **10A** and therefore likely contributing to its increased potency and/or specificity (Figure 6). Each inhibitor achieved the full complement of interactions within the phosphate and

purine binding sites despite their structural dissimilarity. Most of the interactions were preserved by modest perturbations of the amino acid sidechains and slight differences in the orientation of the base. Hydrogen bonds to the 5'-oxygen of AMP and its ribose were replaced in **3** and **10A** by an electrostatic interaction with the furanyl oxygen and by van der Waals interactions between the alkyl substituent(s) and a hydrophobic surface adjacent to the region occupied by the ribosyl moiety of AMP. Despite the large structural differences between **10A** and AMP and the corresponding differences in binding site interactions, **10A** proved to be a fully functional AMP mimic capable of binding to the allosteric AMP binding site and inducing the same protein conformational change as AMP that converts the catalytically active R-form to the inactive T-form.⁴⁰ Furthermore, **10A** reached the same maximal inhibition as AMP (~99%) and like AMP achieved this over a relatively narrow concentration range ($\text{IC}_{10} = 4 \text{ nM}$ and $\text{IC}_{90} = 60 \text{ nM}$). Last, like AMP, **10A** inhibited FBPase synergistically with fructose 2,6-bisphosphate.^{41,18}

In contrast to AMP and closely related AMP analogs, **10A** discriminated between the AMP site of FBPase and AMP binding sites of other enzymes. High FBPase specificity was achieved by exploiting interactions available in the FBPase site that are unique to FBPase and by avoiding binding interactions commonly used by other AMP binding sites.⁴² More specifically, **10A** forms favorable electrostatic interactions with the thiazole nitrogen, amino group, and furanyl spacer oxygen as well as van der Waals interactions with the *i*-butyl group. In contrast, AMP in sites other than FBPase commonly forms hydrogen bonds with the pyrimidine nitrogens, N1 and/or N3, as well as with either or both of the ribosyl hydroxyls. The high specificity of **10A** was also attributed to differences in the preferred AMP binding conformation, which as defined by the torsion angles corresponding to the glycosidic bond ($\chi = -153^\circ$), ribose pucker [γ ($\text{O}_5'-\text{C}_5'-\text{C}_4'-\text{C}_3'$) = 64°] and 5'-phosphate orientation [β ($\text{P}-\text{O}_5'-\text{C}_5'-\text{C}_4'$) = -140°] can vary widely across AMP binding sites. Accordingly, few sites other than FBPase are expected to readily accommodate molecules that link the base to the PO_3^{2-} group by a furanyl spacer group.¹⁷

One finding not readily apparent from the structure or initial modeling studies was the high dependence of inhibitory potency on the 5-membered heterocycle. The 2-aminoimidazole analog substituted with an alkyl group at C5 represented the closest structural analog to the initial lead inhibitor **3** that lacked the second aryl ring. Replacement of the imidazole in **15A** with an oxazole (**13A**) or a thiazole (**10A**) led, respectively, to a 42- and 312-fold improvement in relative binding affinity. *Post hoc* FEP calculations attributed the improvement to decreased desolvation costs. FEP calculations also supported the experimental observations suggesting that the substituents on the

(38) Potential glucose lowering mechanisms for metformin. Hepatic effects: (a) Argand, D.; Roth, H.; Wiernsperger, N.; Lerve, X. M. *Eur. J. Biochem.* **1993**, *213*, 1341–1348. (b) Cleasby, M. E.; Dzamko, N.; Hegarty, B. D.; Cooney, G. J.; Kraegen, E. W.; Ye, J. M. *Diabetes* **2004**, *53*, 3258–3266. (c) Perriello, G.; Misericordia, P.; Volpi, E.; Santucci, A.; Santucci, C.; Ferrannini, E.; Ventura, M. M.; Santeusanio, F.; Brunetti, P.; Bolli, G. B. *Diabetes* **1994**, *43*, 920–928. (d) Zhou, G.; Myers, R.; Li, Y.; Chen, Y.; Shen, X.; Fenyk-Melody, J.; Wu, M.; Ventre, J.; Doebber, T.; Fujii, N.; Musi, N.; Hirshman, M. F.; Goodyear, L. J.; Moller, D. E. *J. Clin. Invest.* **2001**, *108*, 1167–1174. Non-hepatic effects: (e) Radziuk, J.; Bailey, C. J.; Wiernsperger, N. F.; Yudkin, J. S. *Curr. Drug Targets Immune Endocr. Metabol. Disord.* **2003**, *3*, 151–169.

(39) (a) El-Mir, M. Y.; Nogueira, V.; Fontaine, E.; Averet, N.; Rigoulet, M.; Lerve, X. *J. Biol. Chem.* **2000**, *275*, 223–228. (b) Owen, M. R.; Doran, E.; Halestrap, A. P. *Biochem. J.* **2000**, *348* (Pt 3), 607–614.

(40) (a) Ke, H. M.; Liang, J. Y.; Zhang, Y. P.; Lipscomb, W. N. *Biochemistry* **1991**, *30*, 4412–4420. (b) Ke, H. M.; Zhang, Y. P.; Lipscomb, W. N. *Proc. Natl. Acad. Sci. U.S.A.* **1990**, *87*, 5243–5247. (c) Gidh-Jain, M.; Zhang, Y.; van Poelje, P. D.; Liang, J. Y.; Huang, S.; Kim, J.; Elliott, J. T.; Erion, M. D.; Pilkis, S. J.; Raafat el-Maghrabi, M.; Lipscomb, W. N. *J. Biol. Chem.* **1994**, *269*, 27732–27738. (d) Iversen, L. F.; Brzozowski, M.; Hastrup, S.; Hubbard, R.; Kastrop, J. S.; Larsen, I. K.; Naerum, L.; Nørskov-Lauridsen, L.; Rasmussen, P. B.; Thim, L.; Wiberg, F. C.; Lundgren, K. *Protein Sci.* **1997**, *6*, 971–982.

(41) Van Schaftingen, E.; Hers, H. G. *Proc. Natl. Acad. Sci. U.S.A.* **1981**, *78*, 2861–2863.

(42) (a) Moodie, S. L.; Mitchell, J. B.; Thornton, J. M. *J. Mol. Biol.* **1996**, *263*, 486–500. (b) Moodie, S. L.; Thornton, J. M. *Nucleic Acids Res.* **1993**, *21*, 1369–1380.

Table 6. Adenylate Levels and Energy Charge in Isolated ZDF Rat Hepatocytes

	[drug] (μM)	ATP ^a ($\mu\text{mol/g cells}$)	ADP ^a ($\mu\text{mol/g cells}$)	AMP ^a ($\mu\text{mol/g cells}$)	energy charge ^b
control	0	1.35 \pm 0.12	0.37 \pm 0.03	0.12 \pm 0.01	0.833 \pm 0.003
metformin	3000	1.24 \pm 0.05	0.33 \pm 0.02	0.10 \pm 0.01	0.841 \pm 0.005
	10 000	1.06 \pm 0.05 ^c	0.31 \pm 0.02	0.11 \pm 0.01	0.825 \pm 0.008
MB06322	1	1.76 \pm 0.08 ^c	0.39 \pm 0.02	0.11 \pm 0.01	0.864 \pm 0.006 ^c
	10	1.60 \pm 0.07	0.34 \pm 0.01	0.10 \pm 0.01	0.867 \pm 0.005 ^c

^a Adenylates were measured after 1.5 h of drug or vehicle exposure in duplicate samples in three different cell preparations. ^b Energy charge is defined as: $([\text{ATP}] + 1/2 [\text{ADP}])/([\text{ATP}] + [\text{ADP}] + [\text{AMP}])$. ^c $p < 0.05$ vs control: ANOVA, Dunnett's *post hoc* test.

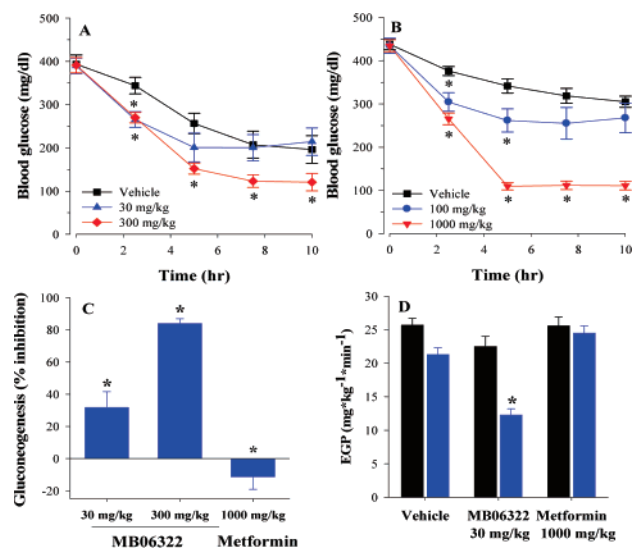


Figure 5. (A–B) Blood glucose lowering following oral administration of (A) MB06322 (30 or 300 mg/kg) or (B) metformin (100 or 1000 mg/kg) relative to vehicle controls. All animals were dosed at 7:00 a.m. and food was withdrawn for the remainder of the protocol. $n = 8/\text{group}$. $*p < 0.05$ vs vehicle, repeated measures ANOVA with Dunnett's *post hoc* test. (C) *De novo* glucose synthesis from ^{14}C -bicarbonate in fasting male ZDF rats following acute administration of MB06322 (30 or 300 mg/kg) or metformin (1000 mg/kg). Results are expressed as % inhibition relative to vehicle-treated animals. $n = 4\text{--}9/\text{group}$. (D) Effects of vehicle, MB06322 (single dose, 30 mg/kg), or metformin (single dose, 1000 mg/kg) treatment on endogenous glucose production in male ZDF rats. Black bars indicate baseline values whereas the blue bars indicate post-treatment values. $n = 6$ or $7/\text{group}$. $*p < 0.05$ vs vehicle, ANOVA with Dunnett's *post hoc* test.

5-membered heterocycle, that is, C5 *i*-butyl group, C2 amino, and C4 furanyl oxygen, contributed to the overall binding affinity. Moreover, results from FEP calculations also agreed with the experimental finding demonstrating that the 5-membered heterocycle could be replaced with a 6-membered heterocycle, namely a phenyl-substituted pyridine, without loss of binding affinity.

Oral delivery of this new FBPsase inhibitor series required the development of novel phosphonate prodrugs, since standard phosphonate prodrugs²¹ failed to achieve oral bioavailabilities of more than 15%. Phosphonic diamides were prepared despite previous efforts showing poor oral bioavailability with another phosphonic acid⁴³ and modest oral bioavailability for aryl phosphonamidate **28**. The result was a significant improvement in oral bioavailability (22–47%). Mechanistic studies suggest the diamide prodrug class undergoes an initial esterase-catalyzed conversion to a transient intermediate such as **32** (could also be biscarboxylate), which, analogous to the previously described

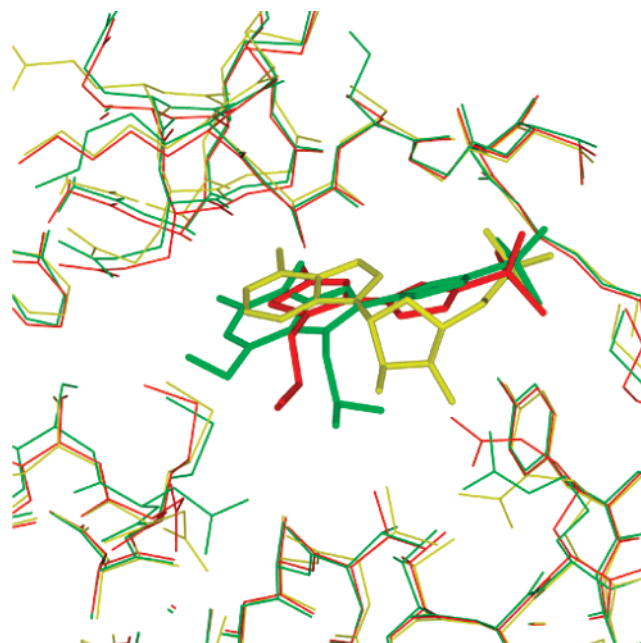


Figure 6. Overlay of human FBPsase complexes containing AMP (yellow), **3** (green), and **10A** (red). The average rms deviation was 0.44 Å for C α and 0.90 Å for the sidechains between the complexes with AMP and **10A**. The average rms deviation was 0.22 Å for C α and 0.85 Å for the sidechains between the complexes with **3** and **10A**.

cleavage mechanism for aryl phosphonamidates,^{35,44} cleaves to the phosphonamidic acid **33** via an intramolecular reaction involving formation of a hydrolytically unstable cyclic intermediate (Scheme 6). The rate of ring closure is likely related to the lability of the leaving group, which could explain the slower conversion rates associated with phosphonic diamides relative to aryl phosphonamidates (Table 5).⁴⁵ Similarly, conversion rates for the diamide prodrug class are slow relative to acyloxyalkyl esters, which, after ester cleavage, breakdown rapidly to the corresponding mono-phosphonic acid and formaldehyde.²⁹ Accordingly, the improved oral bioavailability associated with the phosphonic diamides may relate to the reduced formation of the phosphonamidic acid in the gastrointestinal tract and the inability of the negatively charged mono phosphonic acid to undergo appreciable absorption.

In addition to the improved oral bioavailability, the phosphonic diamide prodrug class exhibits several other potential advantages over standard phosphonate prodrugs. First, phosphonate prodrugs such as acyloxyalkyl esters and substituted

(43) Serafinowska, H. T.; Ashton, R. J.; Bailey, S.; Harnden, M. R.; Jackson, S. M.; Sutton, D. *J. Med. Chem.* **1995**, *38*, 1372–1379.

(44) Jacobsen, N. E.; Bartlett, P. A. *J. Am. Chem. Soc.* **1983**, *105*, 1613–1619.
 (45) An analysis of phosphonamidates as angiotensin converting enzyme inhibitors showed that phenol is a much better leaving group than L-alanyl-L-proline at physiological pH: Galaray, R. E.; Grobely, D. A. *J. Med. Chem.* **1985**, *28*, 1422–1427.

benzyl esters often show significant hydrolytic instability and therefore require additional formulation development and special packaging strategies to achieve adequate shelf life.⁴⁶ The diamide class showed not only good aqueous stability ($t_{90} > 2$ days) but also stability across a broad pH range, which benefits oral absorption by reducing prodrug loss during transit through the gastrointestinal tract.⁴⁷ Second, the diamide class generates nontoxic byproducts, for example, alanine and ethanol, and therefore is associated with a lower toxicological risk than other prodrug classes. Last, the diamides that comprise identical amino acid esters avoid introducing a new stereocenter at phosphorus and the associated synthetic complications.

Conversion of MB06322 to **10A** led to dose-dependent inhibition of GNG in isolated hepatocytes and in the ZDF rat. Inhibition of GNG in the ZDF rat was associated with decreased endogenous glucose production (EGP) and a dose-dependent reduction in blood glucose levels. These results not only demonstrate the importance of GNG to both EGP and the hyperglycemic state of the ZDF rat, but also to the magnitude in which both EGP and glucose levels can be reduced by FBPase inhibitors. Metformin, the only marketed drug for diabetes whose glucose lowering activity is primarily attributed to reduced EGP,⁵ inhibited GNG in rat hepatocytes, but only at a concentration > 1000 -fold higher than the IC_{50} for MB06322. Moreover, unlike MB06322, inhibition by metformin was accompanied by effects on the cellular redox state. In the ZDF rat, metformin at doses that significantly lowered blood glucose failed to inhibit GNG or reduce EGP after oral administration for a single day (Figure 5) or 14 days (data not shown). These results suggest that in the rat, metformin lowers glucose by a mechanism other than inhibition of EGP.

Conclusions

Transformation of the initial FBPase inhibitor lead,¹⁷ **3**, into a drug candidate suitable for testing the FBPase concept in diabetic animal models and ultimately in human clinical trials proved to be a major endeavor. The low oral bioavailability of the bisPOM prodrug of **3**, that is, **4** (2.4%), was attributed to its high MW, low solubility, and inherent susceptibility to esterase cleavage in the gastrointestinal tract. Accordingly, substantial improvement in the oral bioavailability required changes in both the inhibitor structure and prodrug strategy. The FBPase inhibitor **10A** emerged from efforts to reduce the molecular weight of **3** using structural information and molecular modeling studies to guide analog selection and synthesis. **10A** binds to the AMP binding site and elicits potent FBPase inhibition ($IC_{50} = 16$ nM) despite its structural dissimilarity to AMP. Oral delivery of **10A** was accomplished by successfully using a new phosphonate prodrug class, namely the phosphonic diamide, which not only achieved greater oral bioavailabilities

(22–47%) than the standard phosphonate prodrugs but also avoided several well-known limitations commonly associated with these prodrugs, including byproduct toxicity and aqueous instability. Most importantly, these efforts led to MB06322, a prodrug of **10A** that demonstrated that inhibition of gluconeogenesis via inhibition of FBPase results in dose-dependent inhibition of endogenous glucose production and a reduction in blood glucose levels in the ZDF rat. Given the contribution of endogenous glucose production to hyperglycemia in human diabetes, FBPase inhibitors may represent a promising new class of anti-diabetic agents.

Experimental Procedures

General Methods. All moisture-sensitive reactions were performed under a nitrogen atmosphere using oven-dried glassware and anhydrous solvents purchased and used without further manipulation. TLC was performed on Merck silica gel 60 F₂₅₄ TLC glass plates and visualized with UV light or a suitable stain. Flash chromatography was performed on 230–400 mesh EM Science silica gel 60. Melting points were recorded on a Thomas-Hoover capillary melting point apparatus and are uncorrected. ¹H NMR spectra were recorded on Varian Gemini or Mercury spectrometers operating at 200 or 300 MHz, respectively. Mass spectrometry data were determined at Mass Consortium Corp. (San Diego, CA) or on a Perkin-Elmer Sciex API2000 LC-MS system. Elemental microanalyses were performed by NuMega Resonance Labs, Inc. (San Diego, CA) or by Robertson Microlit Laboratories (Madison, NJ).

[5-(4-Methylpentanoyl)furan-2-yl]phosphonic Acid Diethyl Ester (6). A solution of the 2-furan-2-yl-2-[(3-methyl)butyl]-1,3-dioxolane (see Supporting Information, 300 g, 1.43 mol) in anhydrous THF (700 mL) was treated with *N,N,N',N'*-tetramethylethylene-diamine (TMEDA) (215.5 mL, 1.428 mol), cooled to -45 °C, and treated with a solution of *n*-butyl lithium (2.5 M, 600 mL) in hexane via an addition funnel at a speed that maintained the reaction temperature between -45 and -40 °C. After the addition was complete, the reaction solution was stirred at 0 – 2 °C for 1 h. In a separate flask, a solution of diethyl chlorophosphate (228 mL, 1.11 mol) in anhydrous THF (700 mL) was cooled to -45 °C and treated with the above generated furan anion solution (cooled to -45 °C) via a cannula at a rate that maintained the reaction temperature between -45 and -40 °C. After the addition was complete, the reaction was allowed to warm to room temperature and stir for 2 h. The solvent was then removed *in vacuo*, and the residue partitioned between ethyl acetate (1.1 L) and water (880 mL). The layers were separated, and the aqueous phase was extracted with ethyl acetate (800 mL). The organic extracts were then combined, washed with brine (1 L), dried (MgSO₄), filtered, and concentrated *in vacuo* to give crude {5-[2-[(3-methyl)butyl]-1,3-dioxolan-2-yl]-furan-2-yl}phosphonic acid diethyl ester as a dark-red oil (488 g). The ketal was then dissolved in methanol (856 mL), treated with hydrochloric acid (1 N, 215 mL), and heated at 50 °C. After 12 h, the methanol was removed *in vacuo*, and the resulting dark oil partitioned between ethyl acetate (850 mL) and saturated sodium bicarbonate solution (430 mL). The layers were separated, and the aqueous phase was extracted with ethyl acetate (400 mL). The organic extracts were combined, washed with brine (850 mL), dried (MgSO₄), filtered, and concentrated *in vacuo* to a dark-red oil (414 g), which was purified by vacuum distillation (126 – 145 °C/0.10 Torr) to give **6** as a pale-orange oil (112 g, 61%). ¹H NMR (CDCl₃): δ 7.19 (m, 2H), 4.22 (m, 4H), 2.87 (t, 2H, $J = 6.6$ Hz), 1.61 (m, 3H), 1.39 (m, 6H), 0.97 (d, 6H, $J = 6.6$ Hz).

2-Amino-5-isobutyl-4-[2-(5-diethylphosphono)furan-2-yl]thiazole (10). A suspension of [5-(4-methyl-pentanoyl)-furan-2-yl]phosphonic acid diethyl ester (**6**) (500 g, 1.65 mol) and copper(II) bromide (838 g, 3.76 mol) in anhydrous ethanol (5.5 L) was heated to reflux under nitrogen for 1 h. The reaction was then cooled to room temperature and filtered, and the solid was washed with ethanol (0.5 L). The combined filtrate

- (46) Stability studies on phosphonate prodrugs: (a) Cundy, K. C.; Fishback, J. A.; Shaw, J.; Lee, M. L.; Soike, K. F.; Visor, G. C.; Lee, W. A. *Pharm. Res.* **1994**, *11*, 839–843. (b) Benzaria, S.; Pelicano, H.; Johnson, R.; Maury, G.; Imbach, J.; Aubertin, A.; Obert, G.; Gosselin, G. *J. Med. Chem.* **1996**, *39*, 4958–4965. (c) Cundy, K. C.; Sue, I.; Visor, G. C.; Marshburn, J.; Nakamura, C.; Lee, W. A.; Shaw, J. *J. Pharm. Sci.* **1997**, *86*, 1334–1338. (d) Shaw, J.; Louie, M. S.; Krishnamurthy, V. V.; Arimilli, M. N.; Jones, R. J.; Bidgood, A. M.; Lee, W. A.; Cundy, K. C. *Drug Metab. Dispos.* **1997**, *25*, 362–366. (e) Yuan, L.; Dahl, T. C.; Oliyai, R. *Pharm. Res.* **2000**, *17*, 1098–1103. (f) Meier, C.; Gorbic, U.; Muller, C.; Balzarini, J. *J. Med. Chem.* **2005**, *48*, 8079–8086.
- (47) Phosphoramidates were reported to exhibit good stability across the pH range of 5–8.5: Jacobsen, N. E.; Bartlett, P. A. *J. Am. Chem. Soc.* **1981**, *103*, 654–657.

and washing was concentrated under reduced pressure to an oil, which was dissolved in ethyl acetate (4 L) and quenched with a saturated sodium bicarbonate solution (2.8 L). The resulting mixture was filtered through a Celite pad (washed with ethyl acetate, 0.5 L), and the layers were separated. The aqueous phase was extracted with ethyl acetate (2.5 L), and the organic phases were combined and washed with a saturated solution of ammonium chloride, which was subsequently re-extracted with dichloromethane (2 × 30 mL). The organic extracts were combined, washed with brine (1.2 L), dried (MgSO₄), filtered, and concentrated *in vacuo* to give the crude [5-(2-bromo-4-methylpentanoyl)-furan-2-yl]phosphonic acid diethyl ester as a greenish-yellow oil (587 g, 93%). The bromoketone (1086 g, 2.848 mol) was then dissolved in anhydrous ethanol (4 L), treated with thiourea (219 g, 2.88 mol), and heated at reflux. After 1 h, the reaction mixture was cooled to room temperature, concentrated under reduced pressure, neutralized with saturated sodium bicarbonate (3.5 L), and extracted with ethyl acetate (4 L) followed by dichloromethane (1.5 L), ethyl acetate (2 L), and dichloromethane (0.7 L). The organic extracts were combined, washed with brine (2 L), dried (MgSO₄), and filtered, and the filtrate was concentrated under reduced pressure to give a light-orange solid. The crude solid was crystallized from ethyl acetate to give compound **10** as a yellow solid (738 g, 72%). White needles (EtOAc-hexane). mp 121–123 °C. ¹H NMR (CDCl₃): δ 7.18 (m, 1H), 6.59 (m, 1H), 6.18 (bs, 2H), 4.18 (m, 4H), 2.78 (d, 2H, *J* = 6.6 Hz), 1.85 (m, 1H), 1.33 (t, 6H, *J* = 7 Hz), 0.98 (d, 6H, *J* = 6.6 Hz). [MH]⁺ calcd for C₁₅H₂₃N₂O₄PS: 359. Found: 359. Anal. calcd for C₁₅H₂₃N₂O₄PS: C: 50.27, H: 6.47, N: 7.82. Found, C: 50.25, H: 6.31, N: 7.79.

2-Amino-5-isobutyl-4-[2-(5-phosphono)furanyl]thiazole (10A). A solution of **10** (593 g, 1.65 mol) in anhydrous dichloromethane (3.5 L) was cooled to 5 °C and treated with TMSBr (831 g, 5.42 mol). After stirring at room temperature for 16 h, the reaction mixture was evaporated to dryness to yield a residue that was subsequently dissolved in dichloromethane (2 L) and reconcentrated under reduced pressure. The resulting solid was dissolved and concentrated twice from methanol (2 × 2 L) to afford a foam, which was then partitioned between sodium hydroxide (2 M, 1.8 L) and ethyl acetate (1 L). The layers were separated and the aqueous phase was extracted with ethyl acetate (2 × 1 L). The aqueous phase was concentrated slightly under reduced pressure to remove residual ethyl acetate and diluted with water (0.8 L) and methanol (1.25 L). The resulting orange solution was filtered, and the filtrate was treated with concentrated hydrochloric acid (12 M, 220 mL) until pH = 1. The resulting solid was collected via filtration, washed with water (2 × 0.5 L), and dried under vacuum to give **10A** as an off-white solid (476 g, 95%). mp 200–204 °C. ¹H NMR (DMSO-*d*₆): δ 6.97 (m, 1H), 6.74 (m, 1H), 2.74 (d, 2H, *J* = 6.6 Hz), 1.76 (m, 1H), 0.88 (d, 6H, *J* = 6.6 Hz). [MH]⁺ calcd for C₁₁H₁₅N₂O₄PS: 303. Found: 303. Anal. calcd for C₁₁H₁₅N₂O₄PS: C: 43.71, H: 5.00, N: 9.27. Found, C: 43.64, H: 4.78, N: 9.13.

2-Amino-5-isobutyl-4-[5-[N,N'-bis[(S)-1-ethoxycarbonyl]ethyl]-phosphonodiamido]-2-furanyl]thiazole (30). A suspension of **10A** (50 g, 165 mmol) in anhydrous (CICH₂)₂ (1 L) was treated with SOCl₂ (50 mL, 685 mmol) followed by anhydrous pyridine (1.3 mL, 16 mmol). The resulting mixture was heated to reflux under nitrogen. After 3 h, the reaction solution was cooled and evaporated to give a dark-orange semisolid (70.3 g), which was then dissolved in anhydrous (CICH₂)₂ (0.5 L), cooled to –22 °C, and treated with a solution of L-alanine ethyl ester (96.3 g, 822 mmol) in anhydrous CH₂Cl₂. After stirring for 2 h at room temperature, the solution was evaporated to dryness, and the resulting residue partitioned between ethyl acetate (1 L) and water (400 mL). The layers were separated, and the organic phase was washed with brine (300 mL), dried (MgSO₄), filtered, and evaporated to give a brown-orange sludge, which was purified by flash chromatography (SiO₂, 2 kg, 13 cm ID column, 2, 3, and 4% methanol in EtOAc, gradient elution) to give compound **30** as a pale-orange solid (45.9 g, 55%). mp 165–166.5 °C. ¹H NMR (DMSO-*d*₆): δ 6.95–6.90 (m, 3H), 6.50 (m, 1H), 5.07–4.88 (m, 2H), 4.06–3.71 (m, 6H), 2.77 (d, 2H, *J*

= 6.9 Hz), 1.79 (m, 1H), 1.24–1.10 (m, 12H), 0.90 (d, 6H, *J* = 7.2 Hz). [MH]⁺ calcd for C₂₁H₃₃N₄O₆PS: 501. Found: 501. Anal. calcd for C₂₁H₃₃N₄O₆PS: C: 50.39, H: 6.65, N: 11.19. Found, C: 50.30, H: 6.46, N: 11.07.

FBPase Crystal Growth. The hanging drop method was used to grow crystals of the FBPase–**10A** complex at room temperature. Each drop contained human FBPase purified to homogeneity using the procedure previously described¹⁷ (2 μL, 24 mg/mL) in a solution (pH 7.2) containing 2.7 mM **10A**, 5 mM sodium malonate, 1 mM dithiothreitol, 0.5 mM phenylmethylsulfonyl fluoride, 0.1 mM EDTA, and 2 mM fructose-1,6-bisphosphate that was mixed with 2 μL of 6% (vol/vol) polyethylene glycol 8,000 (PEG-8K)/0.1 M Tris-HCl (pH 8.2), and equilibrated against 1 mL 6% PEG-8K/0.1 M Tris-HCl (pH 8.2). The following day, the resulting crystals were soaked in 20% glycerol/80% crystallographic buffer (6% PEG-8K/0.1 M Tris-HCl, pH 8.2) (vol/vol) for about 5 s and then plunged into liquid nitrogen (77 K) and stored until data collection.

Data Collection and Analysis. The diffraction data were collected at 100 K on beamline F-1 of the Cornell High-Energy Synchrotron Source (CHESS). The crystal was in the space group *P*2₁2₁. One tetramer was present in the asymmetric unit.

A search model was obtained from the PDB code 1FTA.^{40c} Molecular replacement was then carried out by using AMORE.⁴⁸ The model of **10A** was generated by CS Chem3D Pro (<http://www.camsoft.com>) and modified according to the electron density in the simulated annealing omit map, and the conformation of the model was optimized by energy minimization in CS Chem3D Pro. The structure of human liver FBPase complexed with **10A** was refined by using the CNS_SOLVE package.⁴⁹ The model was then visualized and refined against 2*F*_o–*F*_c and *F*_o–*F*_c maps by using the program O.⁵⁰ The stereochemical properties of the intermediate and the final structures were examined by PROCHECK.⁵¹ In the final structure, 88.1% residues were in the most favored regions, 11.2% residues were in additional allowed regions, and 0.7% residues were in generously allowed regions.

Computational Details. All molecular dynamics, molecular mechanics, and free-energy perturbation calculations were carried out with the AMBER program using an all-atom force field⁵² and the SPC/E model potential⁵³ to describe water interactions. Procedures for generating the computer model of the FBPase inhibitor complexes and for developing all force field parameters for nonstandard residues are as described in the previous manuscript.¹⁷ Five- and six-membered heterocycles substituted with 2-furanyl phosphonic acid were evaluated computationally using the three-dimensional structure of the human FBPase–ZMP complex (W. N. Lipscomb, unpublished results). The solvated inhibitor and inhibitor-FBPase complex were energy minimized using a four-stage protocol and the BORN module of the AMBER program.

Free-energy calculations were conducted as previously described.²⁸ Prior to the mutation, the system was minimized using the four-stage protocol followed by an equilibration period using 20 ps of MD simulation and a 2 fs time step. Mutations suitable for the single topology method were conducted using 51 windows with each window comprising 3 ps of equilibration and 6 ps of data collection or a total

(48) Navaza, J. *Acta Cryst.* **1994**, *A50*, 157–163.

(49) Brunger, A. T.; Adams, P. D.; Clore, G. M.; DeLano, W. L.; Gros, P.; Grosse-Kunstleve, R. W.; Jiang, J.-S.; Kuszewski, J.; Nilges, N.; Pannu, N. S.; Read, R. J.; Rice, L. M.; Simonson, T.; Warren, G. L. *Acta Cryst.* **1998**, *D54*, 905–921.

(50) Jones, T. A.; Zou, J.-Y.; Cowan, S. W.; Kjeldgaard, M. *Acta Cryst.* **1991**, *A47*, 110–119.

(51) Laskowski, R. A.; MacArthur, M. W.; Moss, D. S.; Thornton, J. M. *J. App. Cryst.* **1993**, *26*, 283–291.

(52) (a) Weiner, S. J.; Kollman, P. A.; Case, D. A.; Singh, U. C.; Ghio, C.; Alagoha, G.; Profeta, S., Jr.; Weiner, P. K. *J. Am. Chem. Soc.* **1984**, *106*, 765–784. (b) Singh, U. C.; Weiner, P. K.; Caldwell, J. K.; Kollman, P. A.; *AMBER Version 3.0*; University of California at San Francisco: San Francisco, CA, 1986.

(53) (a) Berendsen, H. J. C.; Grigera, J. R.; Straatsma, T. P. *J. Phys. Chem.* **1987**, *91*, 6269–6271. (b) Reddy, M. R.; Berkowitz, M. *J. Chem. Phys.* **1988**, *88*, 7104–7110.

of 479 ps of MD simulation. The double topology method²⁷ was used for mutations involving larger structural changes. In this case, calculations entailed two stages with each stage using 51 windows and each window comprising 3 ps of equilibration and 6 ps of data collection or a total of 938 ps of MD simulation. Each mutation followed the doublewide sampling procedure, and the results reported are based on the averages from the backward and forward simulations of the mutation. Errors were estimated for each window by dividing the window statistics into four groups (in both forward and backward directions) and computing the standard deviation for the indicated free-energy change. The root-mean-square of these window errors are reported as a measure of the statistical uncertainty in the result for each mutation.

Hepatocyte Studies. Hepatocytes from freely feeding male ZDF rats were prepared using the method of Berry and Friend⁵⁴ as modified by Groen et al.⁵⁵ Hepatocytes were suspended at 15 mg/mL (gluconeogenesis) or 60 mg/mL (all other assays) in Krebs bicarbonate buffer supplemented with 20 mM glucose. Reactions were performed in a shaking water bath (37 °C).

Hepatocyte Uptake and Metabolism of Phosphonic Diamides. Compound **30** was added to a concentration of 100 μ M, and aliquots of the cell suspension were removed at various time points over 90 min. The cell suspensions were centrifuged for 5 min (Eppendorf microfuge, 16 000 \times *g*, room temperature). The supernatant was removed and the cell pellet extracted by addition of 60% methanol in water (v/v). The methanolic extracts were clarified by centrifugation and analyzed for **30**, **33**, and **10A** by HPLC as described in the Supporting Information.

Metabolic Effects. Hepatocytes were preincubated with **30** (0.3–30 μ M) or metformin (0.3–10 mM) for 30 min prior to the addition of 10 mM ¹⁴C-lactate (0.25 μ Ci/mol) or 1 mM ¹⁴C-glycerol (0.25 μ Ci/mol). For analysis of glucose production, the supernatants were deproteinated with equal volumes of 3 M Ba(OH)₂ and 3 M ZnSO₄ and incubated with or without hexokinase (2.8 U/mL; Sigma, St. Louis, MO) in the presence of 10 mM ATP (1 h, 37 °C). Anion exchange resin was added to each reaction mixture in a 1:2 ratio (wt/vol), and the slurry was incubated with shaking for 1 h (room temperature). Following removal of the resin by centrifugation, radioactivity in the supernatants was assessed by scintillation counting. ¹⁴C-glucose production was calculated from the difference in counts between non-hexokinase-treated and hexokinase-treated (nonspecific) samples. Half-maximal inhibitory (IC₅₀) values were determined by 4-parameter logistic regression with use of Systat software (Point Richmond, CA). Cell pellets were assayed for intracellular lactate and pyruvate as described.⁵⁶ For adenylate measurements, hepatocyte suspensions were spiked directly into acetonitrile (2:3, vol/vol), clarified by centrifugation, and analyzed via liquid-chromatography tandem mass spectroscopy (LC-MS/MS) (see Supporting Information).

ZDF Rat Studies. Acute glucose lowering was measured in ZDF rats (*ca.* 10 weeks old) that were divided into glucose-matched groups at 7:00 a.m. and dosed orally with MB06322 (30 and 300 mg/kg, suspension) or metformin (100 and 1000 mg/kg, solution) or an equal volume of vehicle (0.5% carboxymethyl cellulose in water). Food was withheld for the remainder of the protocol. Blood glucose was measured at baseline and at regular intervals following treatment using the methods described in the Supporting Information.

De novo glucose production was measured in conscious, fasting, male ZDF rats of *ca.* 11 weeks of age. Rats were instrumented with

tail artery and vein catheters under brief halothane anesthesia.⁵⁷ Food was withheld for the remainder of the protocol. After a 4-hour recovery period, MB06322 (30 or 300 mg/kg), metformin (1000 mg/kg), or vehicle was administered orally followed by an intravenous bolus of ¹⁴C-bicarbonate (0.4 μ Ci/g) 3 h later. After 20 min, blood was obtained from the inferior vena cava under halothane anesthesia, diluted 1:12 in water, and processed for ¹⁴C-glucose content.

The rate of EGP was determined using standard tracer dilution techniques.⁵⁸ Male ZDF rats (10–11 weeks old) were fasted at 8 am and instrumented with tail catheters as described above. Food was withheld for the remainder of the protocol. A 16 μ Ci priming dose of 6-[³H]-glucose was administered intravenously at 1:00 p.m. and followed by a maintenance infusion at a rate of 8 μ Ci/h. Neither blood glucose nor insulin was clamped to better simulate physiological conditions. Baseline arterial blood samples to evaluate the specific activity of blood glucose were obtained at 4:00 and 4:30 p.m. At 5:00 p.m., rats were divided into 3 glucose-matched groups and vehicle, MB06322 (30 mg/kg) or metformin (1000 mg/kg), was administered orally. Additional arterial blood samples were obtained 1.5 and 3 h following administration of the test agent. The specific activity of glucose in arterial blood samples was determined as described.⁵⁸ The rate of EGP was calculated by means of the Steele equation⁵⁹ to compensate for the delivery of tracer to a changing systemic glucose pool.

Statistical Analysis. Results are expressed as means \pm SEM. Statistical significance was determined with the student's *t*-test or analysis of variance (ANOVA; one-way or repeated measures) with Dunnett's *post hoc* test as appropriate. Statview software (SAS Institute, Cary, NC) was employed.

Acknowledgment. We thank Kevin Fan, Yan Liu, Dan Cashion, Zhili Sun, Joe Kopcho, William Schulz, and Jay DaRe for their assistance in compound synthesis; Tim J. Colby, Kathy Effenberger, Michael J. Estes, Meredith Pankop, and Emily Topczewski for characterization of the compounds in the biological assays; Dr. Sridhar Prasad for graphical representations of the binding interactions; and Dr. Scott Hecker for review of the manuscript.

Supporting Information Available: Analytical data and procedures for the preparation of compounds **5**, **7–9**, **11–29**, **9A**, **11A–19A**, **31**, and **33**. Enzyme assays, methods for determining solubility, chemical and biological stability, and oral bioavailability, and analytical methods for prodrugs, prodrug metabolites, and cellular adenylates. Procedure for developing force field parameters for nonstandard residues, as well as procedures for energy minimizations in solvent and the complex and for the development of the computer models of FBPase complexed with **10A**. Complete ref 16d. This material is available free of charge via the Internet at <http://pubs.acs.org>.

JA074871L

- (56) Bergmeyer, H. U. In *Methods of Enzymatic Analysis*; Academic Press: New York, 1974; pp 572–579.
- (57) Koo, S. H.; Flechner, L.; Qi, L.; Zhang, X.; Screation, R. A.; Jeffries, S.; Hedrick, S.; Xu, W.; Boussouar, F.; Brindle, P.; Takemori, H.; Montminy, M. *Nature* **2005**, *437*, 1109–1111.
- (58) Rossetti, L.; DeFronzo, R. A.; Gherzi, R.; Stein, P.; Andraghetti, G.; Falzetti, G.; Shulman, G. I.; Klein-Robbenhaar, E.; Cordera, R. *Metabolism* **1990**, *39*, 425–435.
- (59) Minoura, H.; Takeshita, S.; Yamamoto, T.; Mabuchi, M.; Hirosumi, J.; Takakura, S.; Kawamura, I.; Seki, J.; Manda, T.; Ita, M.; Mutoh, S. *Eur. J. Pharmacol.* **2005**, *519*, 182–190.

(54) Berry, M. N.; Friend, D. S. *J. Cell Biol.* **1969**, *43*, 506–520.

(55) Groen, A. K.; Sips, H. J.; Vervoorn, R. C.; Tager, J. M. *Eur. J. Biochem.* **1982**, *122*, 87–93.